Molecular Therapy
Nucleic Acids
Original Article

Optimized allele-specific silencing of the dominant-negative *COL6A1* G293R substitution causing collagen VI-related dystrophy

Astrid Brull,[1,2] Apurva Sarathy,[1,2] Véronique Bolduc,[1] Grace S. Chen,[1] Riley M. McCarty,[1] and Carsten G. Bönnemann[1]

[1]Neurogenetics and Neuromuscular Disorders of Childhood Section, National Institute of Neurological Disorders and Stroke, National Institutes of Health, Bethesda, MD 20892, USA

Collagen VI-related dystrophies (COL6-RDs) are a group of severe, congenital-onset muscular dystrophies for which there is no effective causative treatment. Dominant-negative mutations are common in *COL6A1*, *COL6A2*, and *COL6A3* genes, encoding the collagen α1, α2, and α3 (VI) chains. They act by incorporating into the hierarchical assembly of the three α (VI) chains and consequently produce a dysfunctional collagen VI extracellular matrix, while haploinsufficiency for any of the *COL6* genes is not associated with disease. Hence, allele-specific transcript inactivation is a valid therapeutic strategy, although selectively targeting a pathogenic single nucleotide variant is challenging. Here, we develop a small interfering RNA (siRNA) that robustly, and in an allele-specific manner, silences a common glycine substitution (G293R) caused by a single nucleotide change in *COL6A1* gene. By intentionally introducing an additional mismatch into the siRNA design, we achieved enhanced specificity toward the mutant allele. Treatment of patient-derived fibroblasts effectively reduced the levels of mutant transcripts while maintaining unaltered wild-type transcript levels, rescuing the secretion and assembly of collagen VI matrix by reducing the dominant-negative effect of mutant chains. Our findings establish a promising treatment approach for patients with the recurrent dominantly negative acting G293R glycine substitution.

INTRODUCTION

Collagen VI-related dystrophies (COL6-RDs) are a comparatively common group of muscular dystrophies with a broad clinical spectrum, ranging from the milder Bethlem myopathy (OMIM: 158810), through intermediate phenotypes, to the severe Ullrich congenital muscular dystrophy (OMIM: 254090). UCMD is characterized by an early-onset generalized progressive muscle weakness and wasting, joint hyperlaxity, progressive contractures, and respiratory dysfunction,[1] for which there is no causative treatment.

Collagen VI is a structural and signaling protein localized in the extracellular matrix that forms a microfibrillar network and interacts with other matrix components. α1(VI), α2(VI), and α3(VI) chains, the three basic collagen VI elements necessary for its production, are encoded by *COL6A1*, *COL6A2*, and *COL6A3* genes, respectively,[2] and are composed of a short Gly-X-Y-enriched triple helical (TH) domain flanked by N-terminal and C-terminal globular domains.[3,4] Collagen VI undergoes a complex multistep assembly process, where the three chains (in a 1:1:1 stoichiometry) initially intertwine through their TH domains to form a heterotrimeric monomer. Monomers associate laterally in an antiparallel manner to form disulfide-bonded dimers, which then parallelly assemble to form tetramers. Tetramers are finally secreted into the extracellular space where they associate in an end-to-end manner to form a beaded microfibrillar network.[5–9]

COL6-RDs are caused by either recessive loss of function or more commonly by *de novo* dominant-negative pathogenic variants in the three main *COL6* genes. *De novo* dominant-negative variants are typically either in-frame exon-skipping variants (found in all three *COL6* genes), a deep intronic variant in *COL6A1* that creates a cryptic splice donor site resulting in an in-frame insertion of a 72-base pair (bp) pseudoexon, or single nucleotide missense variants causing glycine substitutions that interrupt the Gly-X-Y motif of the TH domain.[1,10–14] All three variant classes are common pathogenic mechanisms in dominant COL6-RD, with some individual recurrent variants causing the most cases.[11,15,16] Glycine substitutions, such as the recurrent c.877G>A in *COL6A1* that causes a Gly to Arg substitution in position 293 (henceforth designated as G293R), cluster in Gly-X-Y triplets 3–20 at the N-terminal end of the TH domain and have a severe dominant-negative effect due to their ability to produce a stable but deformed helix able to retain the mutant chain in the monomer, and subsequently in the tetramer.[17,18] Consequently, mutant tetramers are trapped in the secretory pathway, causing a reduction of collagen VI in the extracellular matrix, and/or they are secreted

Received 26 September 2023; accepted 19 March 2024;
https://doi.org/10.1016/j.omtn.2024.102178.

[2]These authors contributed equally

Correspondence: Carsten G. Bönnemann, MD, Neurogenetics and Neuromuscular Disorders of Childhood Section, National Institute of Neurological Disorders and Stroke, National Institutes of Health, Bethesda, MD 20892, USA.
E-mail: carsten.bonnemann@nih.gov

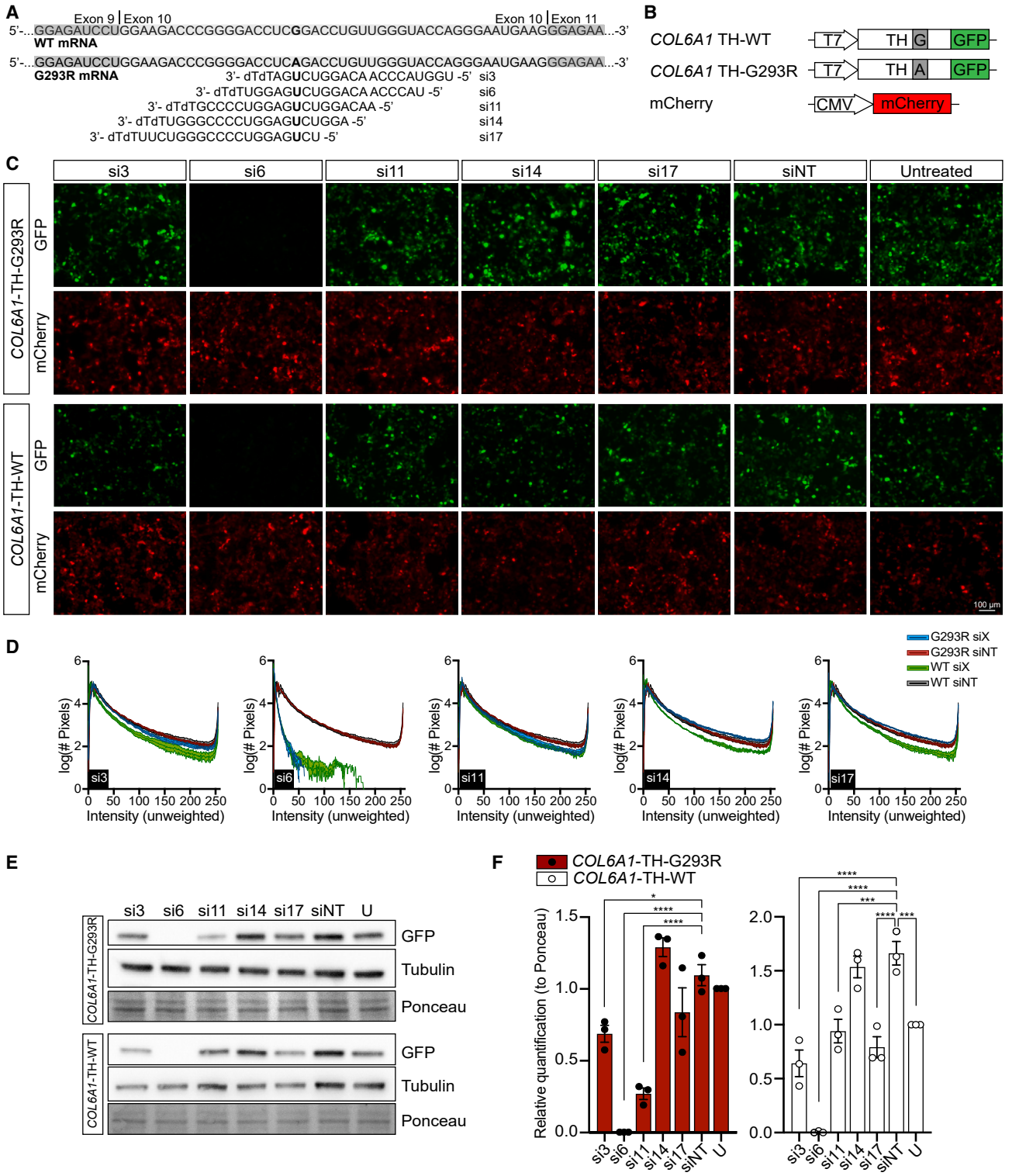

Figure 1. Design and screening of siRNAs targeting the missense *COL6A1* c.877G>A (G293R) pathogenic variant

(A) Schematic representation of wild-type and mutant *COL6A1* exon 10 mRNA sequences and the screened antisense siRNA sequences targeting the *COL6A1* c.877G>A (G293R) pathogenic variant.(B) Schematic representation of the reporter constructs used in the study.(C) Representative live images of HEK293T cells after 48-h

(legend continued on next page)

into the extracellular space but have reduced ability of associating with other tetramers, resulting in disturbance of collagen VI matrix assembly and function.[10,19]

Losing expression from one copy of any of the three *COL6* genes is not disease causing for COL6-RD (i.e., the genes are haplosufficient),[20–23] therefore the use of antisense oligonucleotides or siRNAs to allele-specifically silence mutant transcripts or the use of CRISPR-Cas9-mediated allele-specific gene editing have been explored as therapeutic approaches for COL6-RD.[12,24–29] However, efficacy of allele-specific silencing is highly sequence dependent and single nucleotide substitutions pose a particular challenge, as the mutant and wild-type (WT) alleles only differ by one nucleotide.

In this study, we explored the potential of allele-specific siRNA knockdown as a therapeutic approach for the dominant-negative G293R pathogenic variant in the *COL6A1* gene, one of the most common glycine substitutions in UCMD.[15]

RESULTS

si6 suppresses the expression of both COL6A1 WT and G293R TH domain reporter constructs

We designed a set of 19 siRNAs that sequentially tile across the human *COL6A1* transcript harboring the missense pathogenic variant G293R. The 19 siRNAs were scored following the eight criteria described by Reynolds et al.[30] (see the materials and methods section and Table S1) and selected siRNAs were screened for their potency and allele specificity (Figure 1A). To test the efficacy and allele specificity of siRNAs, we generated green fluorescent protein (GFP)-fused reporter constructs for both the WT and the mutant (G293R) *COL6A1* TH domains (Figure 1B). At 100 nM, si3, si6, and si11 achieved knockdown of *COL6A1* TH-G293R transcripts compared with a non-targeting siRNA (siNT); si6 being the most efficient siRNA (Figures 1C and 1D). Immunoblots confirmed si6 as the most potent siRNA with a 100% knockdown; however, there was no allele specificity as the expression of both constructs was suppressed when using si3, si6, and si11 (Figures 1E and 1F). The lack of allele specificity was not dose dependent, as similar results were obtained when using a lower dose (10 nM; Figure S1).

Increasing allele specificity of si6 by the introduction of additional mismatches

Introduction of additional single-base mismatches into siRNA has been reported to improve allele-specific silencing by decreasing base-pairing efficiency between siRNA and the WT mRNA due to the now two mismatches, while maintaining binding to the mutant allele with only one mismatch.[31] To enhance allele specificity of si6 while maintaining its efficacy, we thus conducted a second siRNA screening, wherein we introduced single-base mismatches along the si6 sequence (Figure 2A) and we evaluated their effect on suppressing *COL6A1* TH-WT and *COL6A1* TH-G293R construct transcripts using 1 nM of siRNA. Except for si6-9G, si6-10G, and si6-11A (with a 30% ± 3%, 89% ± 2%, and 41% ± 4% knockdown, respectively), the addition of a mismatch did not alter efficacy as all siRNAs achieved knockdown levels of *COL6A1* TH-G293R transcripts comparable to si6 (100% knockdown) (Figure 2B). Allele specificity, by contrast, was greatly enhanced when using si6-9G, si6-10G, si6-11A, and si6-16C; all four siRNAs showing no capacity to knock down *COL6A1*-TH-WT transcripts (0% knockdown; Figures 2B and 3). When increasing siRNA dose to 10 nM (Figures S2 and S3), si6-9G, si6-10G, and si6-11A showed a dose-dependent response, with an increase on *COL6A1* TH-G293R transcript silencing of 56%, 10%, and 49% and reaching total knockdown levels of 86% ± 3%, 99% ± 0%, and 90% ± 2%, respectively. The dose increment also reduced allele specificity, with an increase in *COL6A1* TH-WT transcript silencing when using si6-9G, si6-11A, and si6-16C of 26% ± 11%, 45% ± 5%, and 42% ± 2%, respectively. si6-10G resulted to be the most allele-specific siRNA with very low levels of *COL6A1* TH-WT transcript silencing at 1 nM and 10 nM (0% and 19% ± 14%, respectively), compared with 89% ± 2% and 99% ± 0% *COL6A1* TH-G293R transcript knockdown, respectively. si6-10G and si6-16C were selected for further characterization as they showed efficacy and allele specificity. si6-8U was also selected for further characterization, as this siRNA showed high potency at silencing the *COL6A1* TH-G293R transcripts in the low concentration experiment (Figures 2B and 3) but did not show a clear dose-dependent response in silencing the *COL6A1* TH-WT transcripts (Figures 2B, 3, S2, and S3).

Allele-specific silencing of the dominant-negative G293R transcript results in increased extracellular matrix deposition of collagen VI in patient-derived dermal fibroblasts

The missense pathogenic variant *COL6A1* G293R is known to exert a dominant-negative effect on collagen VI microfibrillar matrix assembly and secretion, resulting in increased intracellular collagen VI retention. From our second siRNA screening using *COL6A1* TH constructs, we selected si6-8U, si6-10G, and si6-16C as the most efficient and allele-specific siRNAs to target *COL6A1* G293R transcripts. To test their efficacy and allele specificity on silencing endogenous mRNA, si6, si6-8U, si6-10G, and si6-16C were transfected using a concentration curve (from 0.0032 nM to 10 nM) into cultured dermal fibroblasts derived from a UCMD patient harboring the G293R pathogenic variant in the *COL6A1* gene (G293R Pt 1). Forty-eight hours after transfection, total RNA was isolated and *COL6A1* WT and G293R transcript levels were measured by quantitative PCR (qPCR;

co-transfection with the corresponding GFP construct and 100 nM siRNA. mCherry construct was used as a transfection control. Scale bar, 100 μm.(D) Fluorescence intensity quantification of GFP expression was measured from three independent co-transfection experiments and lines and filled areas indicate the mean ± SEM. (E) Representative immunoblots of GFP expression in HEK293T cells after 48-h co-transfection with the corresponding GFP construct and 100 nM siRNA. Tubulin and Ponceau are shown as loading controls. (F) Relative quantification of GFP expression, normalized to Ponceau, measured from three independent co-transfection experiments. Bars indicate the mean ± SEM. $^{*}p \leq 0.05$, $^{***}p \leq 0.001$, $^{****}p \leq 0.0001$, Ordinary one-way ANOVA and Dunnett's multiple comparisons test were applied. siNT, non-targeting siRNA; siX, analyzed siRNA; TH, triple helical domain; U, Untreated.

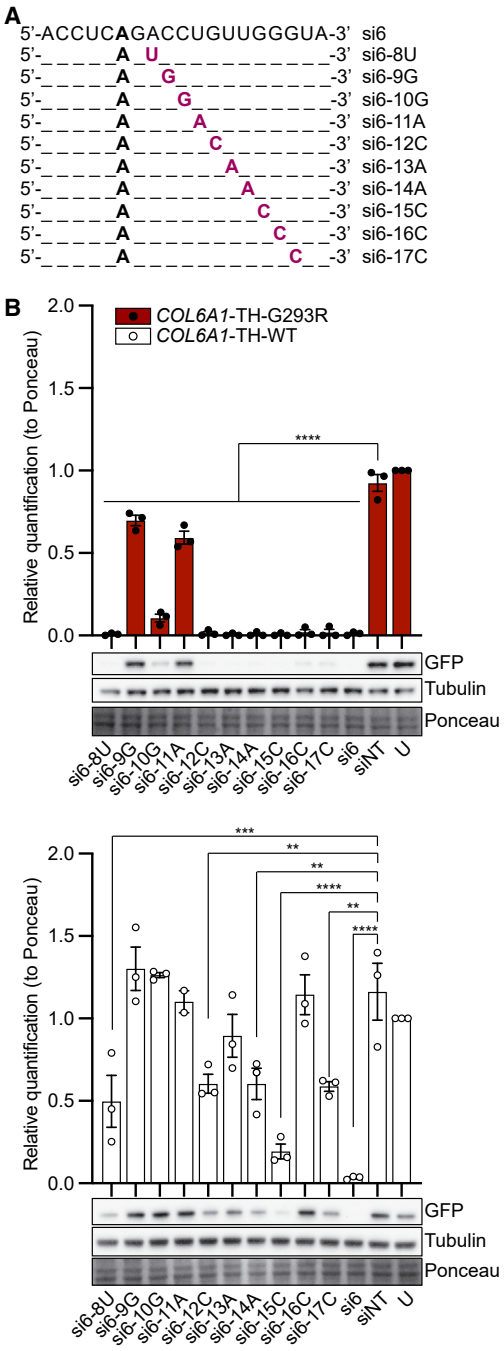

Figure 2. Addition of mismatches to si6 sequence enhances allele specificity

(A) Sense sequence of si6 and si6 with additional mismatches targeting the *COL6A1* c.877G>A (G293R) pathogenic variant.(B) Representative GFP expression immunoblots and relative quantification of GFP expression, normalized to Ponceau, in HEK293T cells at 48 h post-co-transfection of the corresponding GFP construct and 1 nM of siRNA, measured from three independent co-transfection experiments. Tubulin and Ponceau are shown as loading controls. Bars indicate the mean ± SEM. $^{**}p \leq 0.01$, $^{***}p \leq 0.001$, $^{****}p \leq 0.0001$, Ordinary one-way ANOVA and Dunnett's multiple comparisons test were applied. siNT, non-targeting siRNA; U, Untreated.

Figure 4A) using a single nucleotide polymorphism (SNP) cDNA genotyping assay. All tested siRNAs silenced *COL6A1* G293R mRNA in a dose-dependent manner. si6 was also the most potent siRNA knocking down the endogenous *COL6A1* G293R mRNA with a half maximal effective concentration (EC_{50}) of 0.006 nM, followed by si6-8U (0.028 nM), si6-16C (0.040 nM), and si6-10G (0.080 nM; si6 > si6-8U > si6-16C > si6-10G). By contrast, while si6, si6-8U, and si6-16C showed minimal allele specificity, si6-10G was allele specific at all tested concentrations, as shown by the maintained WT mRNA levels in treated dermal fibroblasts derived from a *COL6A1* G293R patient (Figure 4A) as well as from a treated unaffected individual (Figure S4). Although both si6-8U and si6-16C were not allele specific, si6-8U showed slightly better WT vs. G293R allele discrimination than si6-16C (Figure 4A).

To investigate whether specific mutant G293R mRNA silencing translates to a reduction of the mutant protein load allowing for an improved collagen VI matrix secretion and deposition, we analyzed collagen VI matrix after siRNA treatment using an immunofluorescence assay followed by a confocal microscopy-based volumetric analysis of deposited collagen VI matrix (Figures 4B and 4D). Based on the qPCR results, dermal fibroblasts from three patients (G293R Pt 1–3) were treated with si6-8U and si6-10G at two different doses: (1) lower dose with maximum G293R mRNA silencing and maximum G293R vs. WT allele discrimination (0.08 nM [si6-8U] and 0.4 nM [si6-10G]) and (2) minimum dose to achieve maximum G293R mRNA knockdown (all, 2 nM). si6 and siNT at 2 nM were used as positive and negative controls, respectively. Upon quantification, as expected, untreated and siNT-treated G293R Pt 1–3 fibroblasts had reduced collagen VI deposition into the extracellular matrix compared with untreated unaffected individuals (unaffected 1–3; Figure 4B). Moreover, untreated and siNT-treated G293R Pt 1–3 fibroblasts presented discontinuous and speckled collagen VI microfibrils compared with the continuous and linear collagen VI microfibrils observed in untreated unaffected individuals (Figure 4D), resulting in a reduction on collagen VI colocalization with the extracellular matrix protein fibronectin (Figure 4C). In permeabilized samples, collagen VI immunofluorescence revealed intracellular retention of collagen VI immunoreactive material (Figure S5**).** si6-treated G293R fibroblasts presented a complete loss of collagen VI matrix as si6 silenced both WT and G293R mRNA (Figure 4). Treatment with si6-8U at 0.08 nM resulted in a significant increase on collagen VI matrix deposition together with an improvement in collagen VI morphology with more linear and continuous microfibrils. By contrast, due to its non-allele-discriminating nature, si6-8U at 2 nM resulted in a reduction on collagen VI matrix deposition caused by the WT allele unspecific silencing (Figures 4A and 4B). In contrast, si6-10G treatment markedly improved collagen VI matrix deposition and quality with both doses, changes being more pronounced at 2 nM, where collagen VI deposition levels increased significantly and equaled the levels observed in unaffected controls. Matrix appearance was also considerably improved after si6-10G treatment, with thicker and more abundant linear and continuous microfibrils, resembling those observed in the unaffected controls (Figures 4B

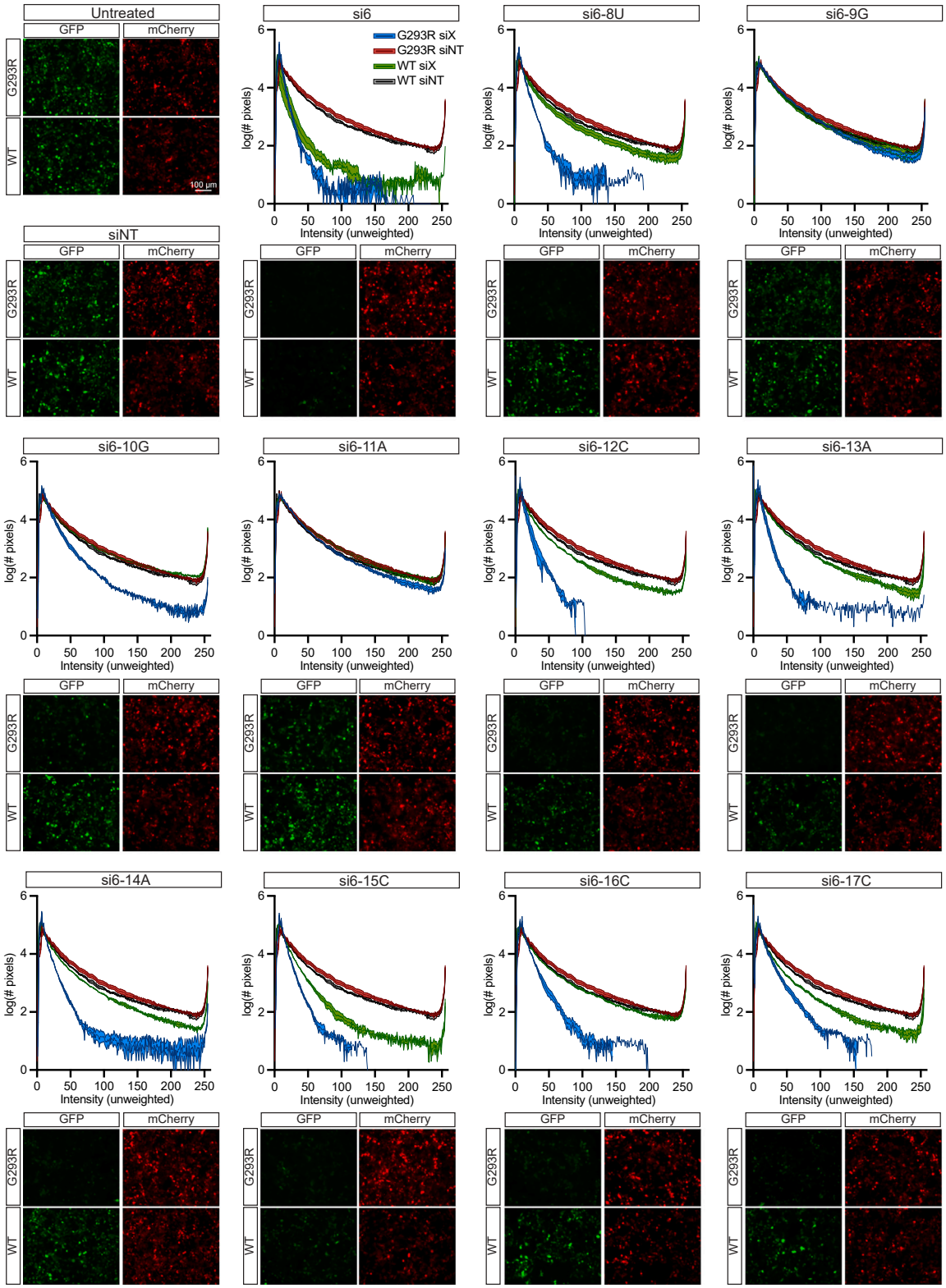

(legend on next page)

and 4D). Both siRNAs significantly increased collagen VI-fibronectin colocalization in the extracellular matrix (Figure 4C) and reduced collagen VI intracellular retention (Figure S5). Therefore, treatment with G293R allele-specific siRNAs appeared to improve both the secretion and microfibrillar assembly of collagen VI matrix by reducing the dominant-negative effect of mutant chains.

DISCUSSION

The observation that carrier parents of UCMD patients with loss-of-function variants present reduced collagen VI production but are still clinically asymptomatic indicates that complete haploinsufficiency for any of the three *COL6* genes is not associated with clinical disease.[20,21,32] Therefore, allele-specific inactivation or knockdown of the mutant allele presents itself as a potential therapeutic strategy for COL6-RD caused by such dominant-negative variants. In the present study, we chose allele-specific RNAi as approach to silence the recurrent *COL6A1* G293R pathogenic variant. Allele-specific siRNA therapies have been explored in other neurodegenerative disorders and muscular dystrophies, including COL6-RD, and in the best case provide robust and specific mutant transcript silencing leading to an improvement of the assessed phenotype.[24,26,33–38] Our current study demonstrates that specifically designed siRNAs can be used to discriminate a single nucleotide difference to target the common G293R missense variant in *COL6A1* in an allele specific manner, mitigating the dominant-negative impact of this variant.

We applied the eight criteria described by Reynolds et al.[30] to select five siRNAs with capability to specifically silence the mutant G293R allele, but none of them exhibited sufficient allele specificity. si6 displayed the highest efficacy with a 100% silencing of both WT and mutant (G293R) protein expression. All designed siRNAs perfectly matched the target mutant sequence but differed in one mismatched single nucleotide with the WT sequence. Previous studies suggest that nucleotide mismatches can prompt RNAi activity,[37,39] but this activity may vary depending upon siRNA thermodynamic properties, suggesting that the specific mismatch position in si6 might favor RNAi activity on the WT transcript. To change thermodynamic properties of si6 and enhance allele discrimination between WT and mutant alleles, we employed the strategy applied by Ohnishi and colleagues[31] to introduce mismatching base substitutions into si6 sequence. Out of the 10 siRNAs with additional mismatches we tested, three (si6-8U, si6-10G, and si6-16C) displayed high efficacy and allele specificity. siRNAs with enhanced allele specificity present modifications in the central position (si6-10G) and in the seed region (si6-16C) of the sense-strand siRNA, in agreement with the key regions to introduce base substitutions proposed by Ohnishi and colleagues and that are related to target RNA cleavage and target RNA recognition. In cultured fibroblasts, si6, si6-8U, si6-10G, and si6-16C induced different levels of efficacy and allele specificity in a dose-dependent manner. While si6 markedly was the most potent siRNA, the addition of a single-base mismatch variably reduced its effectiveness on silencing the mutant allele. The decreased efficacy was, however, compensated by much improved allele specificity. While none of the selected siRNAs resulted in the ideal outcome of complete silencing of the mutant allele with unaltered WT allele levels, two patterns were observed: (1) greater reduction of the mutant transcript along with a partial concomitant WT transcript silencing (si6-8U and si6-16C) and (2) partial mutant transcript silencing but unaltered levels of the WT transcript (si6-10G). Our current data show that allele specificity plays a more important role than overall silencing activity in restoring collagen VI secretion and deposition. si6-8U, at a concentration of 0.08 nM, achieved a 75% knockdown of the mutant transcript with minimal effect on the WT transcript levels, restoring the secretion and deposition of collagen VI matrix. By contrast, at a higher dose, while there was a gain in potency, allele specificity was lost, thereby reducing treatment efficacy. si6-10G achieved a maximum 80% knockdown of the mutant transcript and maintained allele specificity up to a concentration of 10 nM, indicating a broader therapeutic range. The minimum ratio of mutant/WT allele that still results in improvement of the matrix remains to be determined; however, our results indicate that a complete knockdown is not necessary to restore collagen VI secretion and deposition. It is possible that the WT α1(VI) chain that can now assemble without interference from the mutant chain will lead to cumulative correction of the matrix. Additionally, individuals with a mild Bethlem phenotype caused by somatic cellular mosaicism for dominant-negative severe UCMD variants have been reported by our group and others,[40,41] suggesting that even a partial reduction of the mutant transcript would still be clinically beneficial by reverting the severe UCMD phenotype toward a milder Bethlem phenotype.

In conclusion, our study demonstrates that using an optimized design strategy as applied here, siRNAs can efficiently discriminate between single nucleotide variants in *COL6A1* transcripts, thus establishing allele-specific RNAi as a promising molecular approach for the treatment of dominant COL6-RD caused by single nucleotide changes. Numerous improvements in siRNA design, sequence selection, chemical formulation, and delivery mechanisms have been achieved since the discovery of RNAi in 1998.[42–46] RNA-based therapeutic approaches have experienced a surge in the past decade with several RNA drugs being approved by the US Food and Drug Administration for the treatment of neurological and neuromuscular disorders, including antisense oligonucleotides for spinal muscular atrophy[47] and Duchenne muscular dystrophy[48–51] and in August 2018, the first RNAi-based drug for hereditary transthyretin amyloidosis.[52] Hence, with the appropriate chemical modifications to increase stability

Figure 3. Addition of mismatches to si6 sequence increases allele specificity - Continuation

Representative live images and fluorescence intensity quantification of HEK293T cells after 48-h transfection with the corresponding GFP construct and 1 nM siRNA. mCherry construct was used as a transfection control. Fluorescence intensity quantification of GFP expression was measured from three independent experiments and lines and filled areas indicate the mean ± SEM. siNT, non-targeting siRNA; siX, analyzed siRNA; U, Untreated. Scale bar, 100 μm.

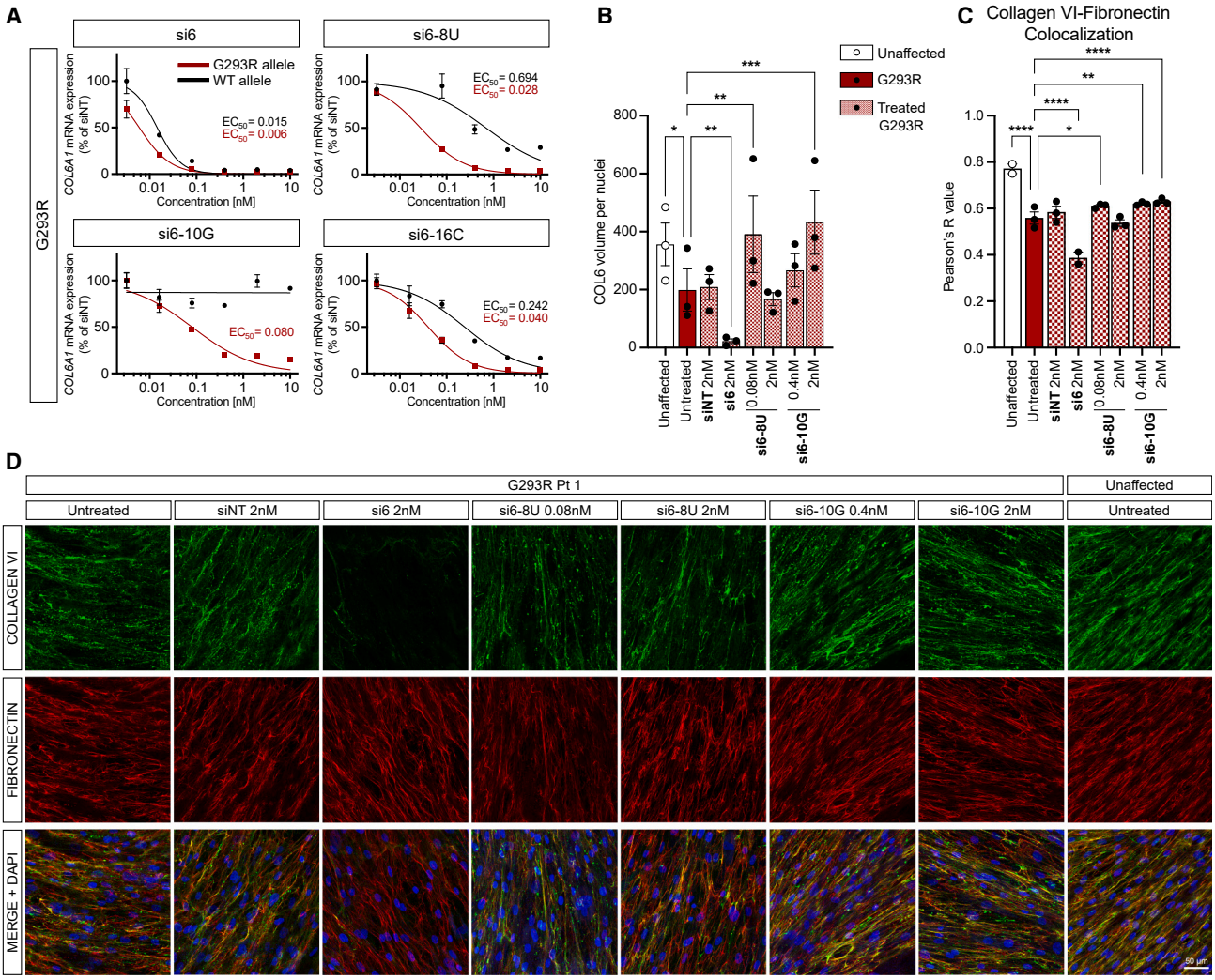

Figure 4. Allele-specific silencing of the G293R mRNA increases collagen VI matrix deposition in patient-derived dermal fibroblasts

(A) Mutant and wild-type *COL6A1* mRNA transcript levels in *COL6A1* G293R patient dermal fibroblasts 48 h post-transfection with a dose curve (0.0032, 0.016, 0.08, 0.4, 2, and 10 nM) of si6, si6-8U, si6-10G, and si6-16C. An SNP genotyping assay was used to discriminate between the mutant and the wild-type allele. *COL6A1* mRNA levels were normalized to *RPLP0*. The experiment was performed in triplicate and bars indicate the mean ± SEM. (B) Total collagen VI volume in the matrix was quantified in each image by measuring the sum of the volume of all objects displaying a longest axis greater than 25 µm, using Volocity 3D Image Analysis Software. Total volume was normalized by the number of nuclei in each image and plotted as a scatter dot plot. Each point corresponds to the mean of three different images of one biological replicate. Bars indicate the mean ± SEM. $^{*}p \leq 0.05$, $^{**}p \leq 0.01$, $^{***}p \leq 0.001$, two-way ANOVA and Dunnett's multiple comparisons tests were applied. (C) Quantification of collagen VI and fibronectin colocalization using the Pearson's correlation coefficient (PCC). Each point corresponds to the mean of 3–7 different images of one biological replicate. Bars indicate the mean ± SEM. $^{*}p \leq 0.05$, $^{**}p \leq 0.01$, $^{****}p \leq 0.0001$, two-way ANOVA and Dunnett's multiple comparisons tests were applied. (D) Representative images of collagen VI and fibronectin matrix immunofluorescence analysis in unaffected and siRNA-treated G293R patient dermal fibroblasts after 7 days with L-ascorbic acid supplementation and three transfections. Stacks of confocal microscopy images were acquired and are presented as a merge. Scale bar, 50 µm. siNT, non-targeting siRNA.

and enhance the delivery to interstitial fibroblasts, our target cells, the next step will be to bring the siRNAs tested in this study into preclinical studies using an appropriate animal model. We are in the process of generating a humanized mouse model harboring the G293R in a partially humanized *Col6a1* gene as a model of the human UCMD variant studied here. This model will allow us to demonstrate the capability of RNAi, as well as other molecular approaches, to treat dominant-negative variants in COL6-RD *in vivo*.

MATERIALS AND METHODS

UCMD patient samples

Three patients (G293R Pt 1–3) harboring the *COL6A1* c.877G>A (G293R) pathogenic variant and three unaffected controls (Unaffected 1–3) were used in the study.

Dermal fibroblast cultures were established from skin biopsies obtained based on standard operating procedures (12-N-0095,

approved by the institutional review board of the National Institute of Neurological Disorders and Stroke [NINDS]). Informed consents were obtained from each individual.

siRNA rational design and selection

Nineteen siRNAs sequentially tiled across the region of the transcript harboring the *COL6A1* c.877G>A (G293R) pathogenic variant were scored based on rules described by Reynolds et al.[30] (Table S1). Each siRNA (sense strand) was assigned a score according five positive characteristics and two negative characteristics associated with siRNA functionality: (1) 36%–53% G/C content, (2) number of "A/U" bases at positions 15–19, (3) absence of internal repeats (T_m <20°C, potential internal hairpin), (4) an "A" base at position 19, (5) an "A" at position 3, (6) a "U" at position 10, (7) a base other than "G" or "C" at position 19, (8) a base other than "G" at position 13. Assigned points for each criterion are shown in Table S1. The highest-scored siRNA oligos (highlighted in gray) were assayed for gene silencing and allele specificity (Figure 1A, and Table S1). Previous studies demonstrated that a mismatch at sense-strand position 19 has very low contribution to target specificity,[53,54] hence si19 was excluded from the study even though it obtained one of the highest scores. Additionally, despite its low score, si14 was also added to the study because of its mismatch position with the WT transcript located at the seed region. For siRNAs with additional mismatches, single-based mismatches were introduced throughout the si6 sense sequence from position 8 to position 17 maintaining equal G/C content. siRNA duplexes were stabilized by the introduction of two dT overhangs at the 3′ end of each 19-mer.[55] siRNAs were synthesized by Dharmacon, Inc. (Lafayette, CO). On-TARGETplus Non-targeting Control siRNA #1 (Catalog ID D-001810-01-05, Dharmacon, Inc., Lafayette, CO) was used as a negative control.

Reporter constructs

We generated GFP-fused reporter constructs for *both COL6A1* WT and G293R mutant TH domains. Total RNA was isolated from patient and unaffected adherent cultured primary dermal fibroblasts using TRIzol Reagent (ThermoFisher Scientific, Carlsbad, CA) according to the manufacturer's instructions and reverse transcribed using Superscript IV kit (ThermoFisher Scientific). A 393-bp region for each genotype was PCR amplified using forward primer 5′- GTAATGGTGTGCTGCTCCTTC GAAT-3′ and reverse primer 5′-GCCCTTTTCTCCTTTCAGTC-3′. PCR products were then gel purified using QIAquick gel extraction kit (Qiagen, Germantown, MD) and cloned into pcDNA6.2/C-EmGFP-GW/TOPO (ThermoFisher Scientific; K35920). Both *COL6A1* TH-WT and G293R reporter constructs were sequence verified by Sanger sequencing (Genewiz, South Plainfield, NJ). The size of the resulting fusion peptide is ∼42 kDa. The mCherry plasmid used as a transfection control was obtained from the Fischbeck lab (NINDS), where dsRed2 in the pBI-CMV4 bidirectional promoter vector was digested and replaced by mCherry.[56]

Cell culture and transfection

HEK293T cells and primary dermal fibroblasts were cultured in Dulbecco's modified Eagle's medium (DMEM) supplemented with 10% fetal bovine serum (FBS) and 1% penicillin/streptomycin at 37°C under 5% CO_2. For reporter constructs transfection experiments, HEK293T cells were co-transfected using Lipofectamine 2000 (ThermoFisher Scientific), according to the manufacturer's transfection protocol, with 1 μg of the *COL6A1* TH-WT or G293R reporter construct, 0.25 μg of the mCherry construct (transfection control), and siRNAs at a final concentration of 100, 10, or 1 nM. Primary dermal fibroblasts were transfected with siRNAs using Lipofectamine RNAiMax (ThermoFisher Scientific) according to the manufacturer's transfection protocol.

Live fluorescent imaging and western blotting

Forty-eight hours after co-transfection of siRNAs and reporter construct DNAs into HEK293T cells, the fluorescence signal emanating from the WT, mutant G293R-TH-GFP fusion protein, or mCherry was observed and recorded with a sCMOS pco.edge 4.2 LT camera (Excelitas Technologies Corp., Wilmington, DE) mounted on an inverted microscope (Nikon Eclipse Ti, Nikon Instruments, Tokyo, Japan). mCherry construct was used as a transfection control. GFP fluorescence intensity was quantified using FIJI software and plotted as the logarithm of the number of pixels vs. fluorescence intensity. To quantify fluorescence intensity, GFP signal was selected using the color threshold tool and measured using the histogram measure tool of FIJI software. Fluorescence intensity quantification of GFP expression was measured from three independent co-transfection experiments. For each replicate, two fields were analyzed and the mean of the two fields was plotted. HEK293T cells were then harvested with RIPA buffer (ThermoFisher Scientific) containing 1x Complete Protease Inhibitor cocktail (MilliporeSigma, Rockville, MD) and 1x PhosSTOP (MilliporeSigma, Rockville, MD). Samples were incubated on ice for 5 min, then spun for 15 min at 14,000 × *g* at 4°C, and supernatant was collected. Protein concentrations were determined using Pierce BCA protein assay kit (ThermoFisher Scientific). Lysates were processed for immunoblotting with rabbit polyclonal anti-GFP antibody (ab290; Abcam, Waltham, MA) and anti-tubulin antibody (T5168, MilliporeSigma, Rockville, MD). Quantification of protein expression was measured from the immunoblot images using the integrated density measure tool of FIJI software. GFP expression was normalized to Ponceau (VWR, Bridgeport, NJ).

RNA isolation, RT-PCR, and qPCR

Total RNA was isolated, and cDNA synthesized from adherent cultured primary dermal fibroblasts using Cells-to-CT kit (ThermoFischer Scientific) according to the manufacturer's protocol. The FastStart Universal Probe Master mix (ROX) (MilliporeSigma) was used to perform the qPCR reactions. qPCR primer/probe mix to detect WT and G293R *COL6A1* transcripts was purchased as a Custom Taqman SNP genotyping assay (ThermoFisher Scientific). qPCR reactions were performed in a total volume of 10 μL, with 3 μL of cDNA (dilution of 1/50 in RNAse-free water). qPCR reactions were run in duplicate on the QuantStudio 6 Flex Real-Time PCR system (Applied Biosystems/ ThermoFisher Scientific, Carlsbad, CA). Ct values were determined

by the QuantStudio Real-Time PCR software (Applied Biosystems/ThermoFisher Scientific). The comparative Ct (ΔΔCt) method was applied to measure the relative expression, using Ribosomal Protein Lateral stalk subunit P0 (*RPLP0*) TaqMan gene expression assay (ThermoFisher Scientific; Hs00420895_gH) Ct values as the endogenous normalizing gene, and the ΔCt values from the siNT-treated controls as the normalizing value.

Matrix immunofluorescence

Patient-derived dermal fibroblasts were seeded (1.5×10^4 cells per well) in eight-chamber tissue culture slides (Corning/ThermoFisher Scientific, Carlsbad, CA). The next day, medium was replaced with DMEM supplemented with 10% FBS and 50 μg/mL of L-ascorbic acid (Wako Chemicals USA, Richmond, VA) and cells were transfected with siRNAs using Lipofectamine RNAiMax (ThermoFisher Scientific). Every 48–72 h, medium was changed, and cells were re-transfected with siRNAs. After 7 days in L-ascorbic supplementation and three siRNA transfections, cultures were fixed with 4% PFA (Electron Microscopy Sciences, Hatfield, PA) for 10 min and rinsed twice in phosphate-buffered saline (PBS). For staining, cells were blocked with 10% FBS in PBS (±0.1% Triton X-100 [T9284, MilliporeSigma]) for 1 h and incubated with anti-collagen type VI antibody (MAB1944; MilliporeSigma) or anti-fibronectin (F3648, MilliporeSigma) in blocking buffer (±0.1% Triton X-100) for 1 h at room temperature. Cells were washed three times with PBS (±0.1% Triton X-100) and incubated with secondary antibody Alexa Fluor 488 goat anti-mouse immunoglobulin (Ig)G (H + L) (A11001, Invitrogen/ThermoFisher Scientific, Carlsbad, CA) or Alexa Fluor 568 goat anti-rabbit IgG (H + L) (A11036, Invitrogen/ThermoFisher Scientific) diluted in blocking buffer (±0.1% Triton X-100) for 1 h at room temperature. Cells were washed again with PBS (±0.1% Triton X-100) and incubated with 4′,6-diamidino-2-phenylindole, dihydrochloride (DAPI) diluted in PBS for 1 min. Cells were washed twice with PBS and mounted with Fluoromount-G (SouthernBiotech, Birmingham, AL).

Confocal imaging and analysis

For matrix quantification, stack images were acquired on a TCS SP5 II or a Stellaris 8 system (Leica Microsystems, Buffalo Grove, IL), with ×40 objective. The pinhole was set to 1 Airy unit and stacks were acquired using either 1.5-μm-sized or system optimized steps. Stacks were merged. To quantify the collagen VI matrix, images were imported into Volocity 3D Image Analysis Software, version 6.1 (PerkinElmer, Waltham, MA). The Find Objects tool was used to filter objects of long axis (by using the longest axis threshold of 25 μm). The collagen VI matrix was quantified as the sum of the volume (μm^3) and normalized by the number of nuclei in each image. The built-in Coloc2 plugin of FIJI software was used to evaluate the colocalization of collagen VI and fibronectin proteins using the Pearson's correlation coefficient (PCC).

Statistics

Graphics and statistical analyses were performed with GraphPad Prism version 9.4.1 (GraphPad Software, San Diego, CA). Data are presented as mean and standard error of the mean (SEM). Performed statistical analysis for each graph is indicated in the corresponding figure legend. $p < 0.05$ was considered as statistically significant.

DATA AND CODE AVAILABILITY

This study includes no data deposited in external repositories.

SUPPLEMENTAL INFORMATION

Supplemental information can be found online at https://doi.org/10.1016/j.omtn.2024.102178.

ACKNOWLEDGMENTS

This study was supported by intramural funds from NINDS (1ZIANS003129) to C.G.B. and by a grant from Fundación Noelia, as well as by funding and support from Cure CMD. The content is solely the responsibility of the author(s) and does not necessarily represent the official views of the National Institutes of Health.

AUTHOR CONTRIBUTIONS

Conceptualization, C.G.B., A.S., V.B.; Methodology, A.B., A.S., and V.B.; Investigation, A.B., A.S., V.B., G.S.C., and R.M.M.; Writing – Original Draft, A.B.; Writing – Review & Editing, A.B., A.S., V.B., C.G.B.; Funding Acquisition, A.S., V.B., and C.G.B.

DECLARATION OF INTERESTS

The authors declare no competing interests. The graphical abstract was created with BioRender.com.

REFERENCES

1. Bönnemann, C.G. (2011). The collagen VI-related myopathies: Muscle meets its matrix. Nat. Rev. Neurol. *7*, 379–390.
2. Weil, D., Mattei, M.G., Passage, E., N'Guyen, V.C., Pribula-Conway, D., Mann, K., Deutzmann, R., Timpl, R., and Chu, M.L. (1988). Cloning and chromosomal localization of human genes encoding the three chains of type VI collagen. Am. J. Hum. Genet. *42*, 435–445.
3. Chu, M.L., Conway, D., Pan, T.C., Baldwin, C., Mann, K., Deutzmann, R., and Timpl, R. (1988). Amino acid sequence of the triple-helical domain of human collagen type VI. J. Biol. Chem. *263*, 18601–18606.
4. Chu, M.L., Pan, T.C., Conway, D., Saitta, B., Stokes, D., Kuo, H.J., Glanville, R.W., Timpl, R., Mann, K., and Deutzmann, R. (1990). The Structure of Type VI Collagen. Ann. N. Y. Acad. Sci. *580*, 55–63.
5. Engvall, E., Hessle, H., and Klier, G. (1986). Molecular assembly, secretion, and matrix deposition of type VI collagen. J. Cell Biol. *102*, 703–710.
6. Furthmayr, H., Wiedemann, H., Timpl, R., Odermatt, E., and Engel, J. (1983). Electron-microscopical approach to a structural model of intima collagen. Biochem. J. *211*, 303–311.
7. Lamandé, S.R., Sigalas, E., Pan, T.C., Chu, M.L., Dziadek, M., Timpl, R., and Bateman, J.F. (1998). The role of the alpha3(VI) chain in collagen VI assembly. Expression of an alpha3(VI) chain lacking N-terminal modules N10-N7 restores collagen VI assembly, secretion, and matrix deposition in an alpha3(VI)-deficient cell line. J. Biol. Chem. *273*, 7423–7430.
8. Godwin, A.R.F., Starborg, T., Sherratt, M.J., Roseman, A.M., and Baldock, C. (2017). Defining the hierarchical organisation of collagen VI microfibrils at nanometre to micrometre length scales. Acta Biomater. *52*, 21–32.
9. Baldock, C., Sherratt, M.J., Shuttleworth, C.A., and Kielty, C.M. (2003). The supramolecular organization of collagen VI microfibrils. J. Mol. Biol. *330*, 297–307.

10. Baker, N.L., Mörgelin, M., Peat, R., Goemans, N., North, K.N., Bateman, J.F., and Lamandé, S.R. (2005). Dominant collagen VI mutations are a common cause of Ullrich congenital muscular dystrophy. Hum. Mol. Genet. *14*, 279–293.

11. Briñas, L., Richard, P., Quijano-Roy, S., Gartioux, C., Ledeuil, C., Lacène, E., Makri, S., Ferreiro, A., Maugenre, S., Topaloglu, H., et al. (2010). Early onset collagen VI myopathies: Genetic and clinical correlations. Ann. Neurol. *68*, 511–520.

12. Bolduc, V., Foley, A.R., Solomon-Degefa, H., Sarathy, A., Donkervoort, S., Hu, Y., Chen, G.S., Sizov, K., Nalls, M., Zhou, H., et al. (2019). A recurrent COL6A1 pseudoexon insertion causes muscular dystrophy and is effectively targeted by splice-correction therapies. JCI Insight *4*, e124403.

13. Cummings, B.B., Marshall, J.L., Tukiainen, T., Lek, M., Donkervoort, S., Foley, A.R., Bolduc, V., Waddell, L.B., Sandaradura, S.A., O'grady, G.L., et al. (2016). Improving genetic diagnosis in Mendelian disease with transcriptome sequencing Genotype-Tissue Expression Consortium. Sci. Transl. Med. *5209*, 1–12.

14. Lampe, A.K., Zou, Y., Sudano, D., O'Brien, K.K., Hicks, D., Laval, S.H., Charlton, R., Jimenez-Mallebrera, C., Zhang, R.Z., Finkel, R.S., et al. (2008). Exon skipping mutations in collagen VI are common and are predictive for severity and inheritance. Hum. Mutat. *29*, 809–822.

15. Butterfield, R.J., Foley, A.R., Dastgir, J., Asman, S., Dunn, D.M., Zou, Y., Hu, Y., Donkervoort, S., Flanigan, K.M., Swoboda, K.J., et al. (2013). Position of glycine substitutions in the triple helix of COL6A1, COL6A2, and COL6A3 is correlated with severity and mode of inheritance in collagen vi myopathies. Hum. Mutat. *34*, 1558–1567.

16. Lampe, A.K., and Bushby, K.M.D. (2005). Collagen VI related muscle disorders. J. Med. Genet. *42*, 673–685.

17. Pace, R.A., Peat, R.A., Baker, N.L., Zamurs, L., Mörgelin, M., Irving, M., Adams, N.E., Bateman, J.F., Mowat, D., Smith, N.J.C., et al. (2008). Collagen VI glycine mutations: Perturbed assembly and a spectrum of clinical severity. Ann. Neurol. *64*, 294–303.

18. Pan, T.C., Zhang, R.Z., Sudano, D.G., Marie, S.K., Bönnemann, C.G., and Chu, M.L. (2003). New Molecular Mechanism for Ullrich Congenital Muscular Dystrophy: A Heterozygous In-Frame Deletion in the COL6A1 Gene Causes a Severe Phenotype. Am. J. Hum. Genet. *73*, 355–369.

19. Lamandé, S.R., Mörgelin, M., Selan, C., Jöbsis, G.J., Baas, F., and Bateman, J.F. (2002). Kinked Collagen VI Tetramers and Reduced Microfibril Formation as a Result of Bethlem Myopathy and Introduced Triple Helical Glycine Mutations. J. Biol. Chem. *277*, 1949–1956.

20. Foley, A.R., Hu, Y., Zou, Y., Yang, M., Medne, L., Leach, M., Conlin, L.K., Spinner, N., Shaikh, T.H., Falk, M., et al. (2011). Large Genomic Delitions: A novel cause of Ullrich Congenital Muscular Dystrophy. Ann. Neurol. *69*, 206–211.

21. Camacho Vanegas, O., Bertini, E., Zhang, R.-Z., Petrini, S., Minosse, C., Sabatelli, P., Giusti, B., Chu, M.-L., and Pepe, G. (2001). Ullrich scleroatonic muscular dystrophy is caused by recessive mutations in collagen type VI. Proc. Natl. Acad. Sci. USA *98*, 7516–7521.

22. Higuchi, I., Shiraishi, T., Hashiguchi, T., Suehara, M., Niiyama, T., Nakagawa, M., Arimura, K., Maruyama, I., and Osame, M. (2001). Frameshift mutation in the collagen VI gene causes Ullrich's disease. Ann. Neurol. *50*, 261–265.

23. Peat, R.A., Baker, N.L., Jones, K.J., North, K.N., and Lamandé, S.R. (2007). Variable penetrance of COL6A1 null mutations: Implications for prenatal diagnosis and genetic counselling in Ullrich congenital muscular dystrophy families. Neuromuscul. Disord. *17*, 547–557.

24. Bolduc, V., Zou, Y., Ko, D., and Bönnemann, C.G. (2014). SiRNA-mediated allele-specific silencing of a COL6A3 mutation in a cellular model of dominant ullrich muscular dystrophy. Mol. Ther. Nucleic Acids *3*, e147.

25. Aguti, S., Bolduc, V., Ala, P., Turmaine, M., Bönnemann, C.G., Muntoni, F., and Zhou, H. (2020). Exon-skipping oligonucleotides restore functional collagen VI by correcting a common COL6A1 mutation in Ullrich congenital muscular dystrophy. Mol. Ther. Nucleic Acids *21*, 205–216.

26. Noguchi, S., Ogawa, M., Kawahara, G., Malicdan, M.C., and Nishino, I. (2014). Allele-specific gene silencing of mutant mRNA restores cellular function in ullrich congenital muscular dystrophy fibroblasts. Mol. Ther. Nucleic Acids *3*, e171.

27. Gualandi, F., Manzati, E., Sabatelli, P., Passarelli, C., Bovolenta, M., Pellegrini, C., Perrone, D., Squarzoni, S., Pegoraro, E., Bonaldo, P., and Ferlini, A. (2012). Antisense-Induced Messenger Depletion Corrects a COL6A2 Dominant Mutation in Ullrich Myopathy. Hum. Gene Ther. *23*, 1313–1318.

28. Marrosu, E., Ala, P., Muntoni, F., and Zhou, H. (2017). Gapmer Antisense Oligonucleotides Suppress the Mutant Allele of COL6A3 and Restore Functional Protein in Ullrich Muscular Dystrophy. Mol. Ther. Nucleic Acids *8*, 416–427.

29. López-Márquez, A., Morín, M., Fernández-Peñalver, S., Badosa, C., Hernández-Delgado, A., Natera-de Benito, D., Ortez, C., Nascimento, A., Grinberg, D., Balcells, S., et al. (2022). CRISPR/Cas9-Mediated Allele-Specific Disruption of a Dominant COL6A1 Pathogenic Variant Improves Collagen VI Network in Patient Fibroblasts. Int. J. Mol. Sci. *23*, 4410.

30. Reynolds, A., Leake, D., Boese, Q., Scaringe, S., Marshall, W.S., and Khvorova, A. (2004). Rational siRNA design for RNA interference. Nat. Biotechnol. *22*, 326–330.

31. Ohnishi, Y., Tamura, Y., Yoshida, M., Tokunaga, K., and Hohjoh, H. (2008). Enhancement of allele discrimination by introduction of nucleotide mismatches into siRNA in allele-specific gene silencing by RNAi. PLoS One *3*, e2248.

32. Demir, E., Sabatelli, P., Allamand, V., Ferreiro, A., Moghadaszadeh, B., Makrelouf, M., Topaloglu, H., Echenne, B., Merlini, L., and Guicheney, P. (2002). Mutations in COL6A3 cause severe and mild phenotypes of Ullrich congenital muscular dystrophy. Am. J. Hum. Genet. *70*, 1446–1458.

33. Trochet, D., Prudhon, B., Beuvin, M., Peccate, C., Lorain, S., Julien, L., Benkhelifa-Ziyyat, S., Rabai, A., Mamchaoui, K., Ferry, A., et al. (2017). Allele-specific silencing therapy for Dynamin 2-related dominant centronuclear myopathy. EMBO Mol. Med. *10*, 239–253.

34. Trochet, D., Prudhon, B., Mekzine, L., Lemaitre, M., Beuvin, M., Julien, L., Benkhelifa-Ziyyat, S., Bui, M.T., Romero, N., and Bitoun, M. (2022). Benefits of therapy by dynamin-2-mutant-specific silencing are maintained with time in a mouse model of dominant centronuclear myopathy. Mol. Ther. Nucleic Acids *27*, 1179–1190.

35. Morelli, K.H., Griffin, L.B., Pyne, N.K., Wallace, L.M., Fowler, A.M., Oprescu, S.N., Takase, R., Wei, N., Meyer-Schuman, R., Mellacheruvu, D., et al. (2019). Allele-specific RNA interference prevents neuropathy in Charcot-Marie-Tooth disease type 2D mouse models. J. Clin. Invest. *129*, 5568–5583.

36. Zaleta-Rivera, K., Dainis, A., Ribeiro, A.J.S., Cordero, P., Rubio, G., Shang, C., Liu, J., Finsterbach, T., Parikh, V.N., Sutton, S., et al. (2019). Allele-Specific Silencing Ameliorates Restrictive Cardiomyopathy Attributable to a Human Myosin Regulatory Light Chain Mutation. Circulation *140*, 765–778.

37. Schwarz, D.S., Ding, H., Kennington, L., Moore, J.T., Schelter, J., Burchard, J., Linsley, P.S., Aronin, N., Xu, Z., and Zamore, P.D. (2006). Designing siRNA that distinguish between genes that differ by a single nucleotide. PLoS Genet. *2*, e140–e1318.

38. Giorgio, E., Lorenzati, M., Rivetti di Val Cervo, P., Brussino, A., Cernigoj, M., Della Sala, E., Bartoletti Stella, A., Ferrero, M., Caiazzo, M., Capellari, S., et al. (2019). Allele-specific silencing as treatment for gene duplication disorders: Proof-of-principle in autosomal dominant leukodystrophy. Brain *142*, 1905–1920.

39. Du, Q., Thonberg, H., Wang, J., Wahlestedt, C., and Liang, Z. (2005). A systematic analysis of the silencing effects of an active siRNA at all single-nucleotide mismatched target sites. Nucleic Acids Res. *33*, 1671–1677.

40. D'Amico, A., Fattori, F., Tasca, G., Petrini, S., Gualandi, F., Bruselles, A., D'Oria, V., Verardo, M., Carrozzo, R., Niceta, M., et al. (2017). Somatic mosaicism represents an underestimated event underlying collagen 6-related disorders. Eur. J. Paediatr. Neurol. *21*, 873–883.

41. Donkervoort, S., Hu, Y., Stojkovic, T., Voermans, N.C., Foley, A.R., Leach, M.E., Dastgir, J., Bolduc, V., Cullup, T., de Becdelièvre, A., et al. (2015). Mosaicism for dominant collagen 6 mutations as a cause for intrafamilial phenotypic variability. Hum. Mutat. *36*, 48–56.

42. Fire, A., Xu, S., Montgomery, M.K., Kostas, S.A., Driver, S.E., and Mello, C.C. (1998). Potent and specific genetic interference by double-stranded RNA in Caenorhabditis elegans. Nature *391*, 806–811.

43. Bramsen, J.B., Laursen, M.B., Nielsen, A.F., Hansen, T.B., Bus, C., Langkjoør, N., Babu, B.R., Højland, T., Abramov, M., Van Aerschot, A., et al. (2009). A large-scale chemical modification screen identifies design rules to generate siRNAs with high activity, high stability and low toxicity. Nucleic Acids Res. *37*, 2867–2881.

44. Snead, N.M., Escamilla-Powers, J.R., Rossi, J.J., and McCaffrey, A.P. (2013). 5′ unlocked nucleic acid modification improves siRNA targeting. Mol. Ther. Nucleic Acids *2*, e103.

45. Janas, M.M., Schlegel, M.K., Harbison, C.E., Yilmaz, V.O., Jiang, Y., Parmar, R., Zlatev, I., Castoreno, A., Xu, H., Shulga-Morskaya, S., et al. (2018). Selection of GalNAc-conjugated siRNAs with limited off-Target-driven rat hepatotoxicity. Nat. Commun. *9*, 723.

46. Robbins, M., Judge, A., Liang, L., McClintock, K., Yaworski, E., and MacLachlan, I. (2007). 2′-O-methyl-modified RNAs act as TLR7 antagonists. Mol. Ther. *15*, 1663–1669.

47. (2016). FDA press release on nusinersen approval. https://wayback.archive-it.org/7993/20170110185509/http://www.fda.gov/NewsEvents/Newsroom/PressAnnouncements/ucm534611.htm.

48. (2021). FDA press release on casimersen approval. https://www.fda.gov/news-events/press-announcements/fda-approves-targeted-treatment-rare-duchenne-muscular-dystrophy-mutation-0.

49. (2016). FDA press release on eteplirsen approval. https://www.fda.gov/news-events/press-announcements/fda-grants-accelerated-approval-first-drug-duchenne-muscular-dystrophy.

50. (2019). FDA press release on golodirsen approval. https://www.fda.gov/news-events/press-announcements/fda-grants-accelerated-approval-first-targeted-treatment-rare-duchenne-muscular-dystrophy-mutation.

51. (2020). FDA press release on viltolarsen approval. https://www.fda.gov/news-events/press-announcements/fda-approves-targeted-treatment-rare-duchenne-muscular-dystrophy-mutation.

52. (2018). FDA press release on patisiran approval. https://www.fda.gov/news-events/press-announcements/fda-approves-first-its-kind-targeted-rna-based-therapy-treat-rare-disease.

53. Haley, B., and Zamore, P.D. (2004). Kinetic analysis of the RNAi enzyme complex. Nat. Struct. Mol. Biol. *11*, 599–606.

54. Martinez, J., and Tuschl, T. (2004). RISC is a 5′ phosphomonoester-producing RNA endonuclease. Genes Dev. *18*, 975–980.

55. Elbashir, S.M., Harborth, J., Lendeckel, W., Yalcin, A., Weber, K., and Tuschl, T. (2001). Duplexes of 21-nucleotide RNAs meditae RNA interference in cultured mammalian cells. Nature *411*, 494–498.

56. Winkelsas, A.M., Grunseich, C., Harmison, G.G., Chwalenia, K., Rinaldi, C., Hammond, S.M., Johnson, K., Bowerman, M., Arya, S., Talbot, K., et al. (2021). Targeting the 5′ untranslated region of SMN2 as a therapeutic strategy for spinal muscular atrophy. Mol. Ther. Nucleic Acids *23*, 731–742.